Polymer 99 (2016) 368–375

Contents lists available at ScienceDirect

Polymer

journal homepage: www.elsevier.com/locate/polymer

Molecular dynamics simulation study of a fracture of filler-filled polymer nanocomposites

Katsumi Hagita [a, *], Hiroshi Morita [b], Hiroshi Takano [c]

[a] Department of Applied Physics, National Defense Academy, Kanagawa, 239-8686, Japan
[b] National Institute of Advanced Industrial Science and Technology, Tsukuba, 305-8568, Japan
[c] Faculty of Science and Technology, Keio University, Yokohama, 223-8522, Japan

ARTICLE INFO

Article history:
Received 9 May 2016
Received in revised form
7 July 2016
Accepted 11 July 2016
Available online 13 July 2016

Keywords:
Coarse grained molecular dynamics simulation
Polymer nanocomposite
Filled rubber
Fracture
Nano-voids

ABSTRACT

We investigated a fracture of polymer nanocomposites filled with spherical nanoparticles (NPs). The dependences of the fracture on the interactions between the NPs and polymers were examined by coarse-grained molecular dynamics simulations in a deformed box with a Poisson ratio of 0.4. In order to observe the creation of nanovoids, the interaction among the polymers was set to be attractive. When the NP-polymer interaction is attractive, nanovoids appear in the bulk of polymers. On the other hand, for repulsive NP-polymer interaction, nanovoids are created at the surface between the polymers and NPs. At the same time, segregation of NPs is observed. We found that these behaviors depend on crosslink densities.

1. Introduction

Reinforcement of soft materials is an important issue for the development of highly functional rubber materials, such as fuel-efficient tires or oil-sealing rubber parts [1–4]. Such reinforcement is attained by filling functionalized nanoparticles (NPs), and this is controlled in the mixing process for the NPs. Mostly effective interaction among functionalized NPs and polymers is non-repulsive in order to avoid segregation of NPs. For industrial applications, it is considered that the improvement of NP's functionality is much important for the dispersion of the NPs [5,6]. Inhomogeneity at NP's surface of attractive interaction leads to interesting morphology formation as an isolated NP cluster [6,7]. Although morphology formation of NPs in rubber materials is a key issue for mechanical properties, which is described by stress strain relation, interactions among NPs and polymer are more fundamental on toughness and/or fracture of those materials. The toughness of rubber materials is sometimes understood by the fractures of those materials, which are classified into cohesive or interfacial fractures [8–10]. For example, in the peeling process of a soft pressure-sensitive adhesive, both fracture modes can be found [11,12]. In the fracture process, nanovoids are first derived, which grow to form a microcavity, and finally the material breaks. Therefore, it can be distinguished that the creation and growth processes of nanovoids are key steps in the study of the fracture mechanism, and nanovoids formed during the fracture processes of rubber materials have been the subject of growing interest in the research area of rubber materials.

A nanovoid is defined as a cavity of nano size, which is smaller than a few tens of nanometers. Due to their size, nanovoids are too difficult to detect. Recently, Creton and co-workers have studied nanovoids in the fracture process of carbon black-filled styrene-butadiene rubber by using small-angle X-ray scattering analysis [13]. If the cavity becomes larger than a few microns, it can be observed by using an optical microscope. Nanovoids of 20–40 nm can be detected in the behaviors of two-dimensional scattering patterns, and measurement of the variation in volume by a digital image correlation method. Although nanovoids can be observed, this is limited to static nanovoids; the structures of voids in dynamic processes have not yet been obtained.

To study the dynamic process of polymeric materials, coarse-

* Corresponding author.
E-mail address: hagita@nda.ac.jp (K. Hagita).

http://dx.doi.org/10.1016/j.polymer.2016.07.030

grained molecular dynamics (cgMD) method is used. This can be applied to several kinds of polymeric materials. Recently, significant progress in simulation techniques has been made in both simulation software and computational tools. Using these tools, we have performed cgMD simulation for thousands of filler-filled polymer nanocomposites (PNCs) in a box corresponding to the sub-micron scale [14]. In the cgMD, detailed movements of polymer chains can be observed. Polymer chain behaviors near the NP-Polymers interface and/or crosslink points are very interesting in the viewpoints of both academia and industries. For the case without nanovoids, distributions of coarse-grained particles and bond orientations near the interface have been examined in the previous work [14]. Moreover, preliminary analysis of local polymer chain dynamics by mean square displacement are performed by the authors. For the case with nanovoids near the interfaces, these analyses can not be directly applied because of absence of polymer chains around NPs. Detailed analyses of polymer behaviors near the interfaces are under consideration. Because the examined system is very complex and complicated, we considered that some probing tests are required to reveal molecular-level mechanism. For example, we have plans to investigate effects of connections between NPs and polymers, size and shape of polymers, and their distribution. Studies in these directions are in progress.

In the present study, we investigated the fracture processes of filler-filled rubbers using cgMD simulations. The present studies focus on difference of behaviors of nanovoids due to NP-polymer interaction, although effect of aggregated structure of NPs is important on its mechanics. Thus, we considered well dispersed initial morphology given by a certain hard sphere configuration as the first investigation of successive studies for filler filled polymer networks. Note that some industrial processes are not equilibrium and NPs are forcedly dispersed by mechanical mixing and cross-linking. Therefore, we considered that simulation studies starting from the random configuration of NPs can be justified. We performed uniaxial elongation of PNCs under an NLpT condition with a Poisson ratio of 0.40 in order to develop fundamental analyses and obtain preliminary results prior to large-scale simulations with a Poisson ratio of 0.46. Here, NLpT denotes the number (N) of beads, dimension (L) in the x-direction, pressure (p) in the y- and z-directions, and temperature (T). We considered uniaxial elongating simulation with Poisson ratio 0.40 is suitable in order to understand basic behaviors and develop framework for systematic analyses of filled polymer materials. The value 0.40 can be regarded as central value of filled polymer materials. Poisson ratio of filled rubber and unfilled rubber is 0.46 and 0.49, respectively. Poisson ratio of crystalline polymer are smaller than that of rubber like polymers. Poisson ratio of polystyrene and high density polyethylene is 0.33 and 0.37, respectively. In our simulations, the elongation ratio λ is less than 400%. In the present paper, the elongation ratio λ is defined as the dimensions for λ becoming $(1+\lambda)$ times that before deformation. In actual PNCs, the Poisson ratio is near 0.46, and nanovoids are considered to be observed for an elongation ratio much larger than 200% [13].

In the next section, the methods for cgMD simulation are explained. Stress-strain relations, and snapshots of nanovoids and fillers are presented in Section 3. Mathematical analyses of Betti numbers on the basis of computational homology are given. In the final section, a summary and conclusion are provided.

2. Methods

We used polymer networks filled with spherical NPs on the basis of the Kremer-Grest model [15]. The details of this model have previously been explained [14]. Dynamics of the particles of polymer networks and NPs are described with a Langevin equation. For polymer networks, Lennard-Jones potential and the finite extensible nonlinear elastic (FENE) potential is applied to neighboring particles and bonded particles, respectively. For a model of a spherical NP, we considered that a sphere consists of the same beads as those of polymer chains and forms a fullerene structure C_{20n^2}. In order to make the NP spherical, a harmonic potential is applied to the surface particles from the center of the NP. The system size under a periodic boundary condition (PBC) is smaller than that in previous large-scale cgMD simulations [14]. In the present paper, the number of beads in the polymer parts is 655,360, which is composed of 640 chains with 1024 beads per chain. We used a smaller filler than that in the model proposed in previous studies. The filler consists of 320 surface beads and one center bead. The diameter of the filler is about 5.56 σ and the number of fillers is 256. The volume fraction of the NPs is about 20%. Thus, the dimension of the PBC box, L_{pbc}, before elongation is about 98 σ. It should be noted that the detailed values of L_{pbc} depend on the interaction parameters. In the present work, to create an attractive interaction among polymers, the cutoff length r_{c} of the Lennard Jones (LJ) potentials is set to 2.5 σ as shown in Table 1. The other parameters are the same, except for the interaction between NPs and polymers. The potential function for the interaction of the NP-polymer and NP-NP interactions is given as following function:

$$U_{NP-X}(r) = 4\varepsilon_{NP-X}\left[\left(\frac{\sigma}{r-r_{\mathrm{const}}}\right)^{12} - \left(\frac{\sigma}{r-r_{\mathrm{const}}}\right)^{6} - \left(\frac{\sigma}{r_{\mathrm{c}}-r_{\mathrm{const}}}\right)^{12} + \left(\frac{\sigma}{r_{\mathrm{c}}-r_{\mathrm{const}}}\right)^{6}\right]. \quad (1)$$

Here, constant parameters r_{const} for the NP-polymer and NP-NP interactions are set to $r_{\mathrm{const,NP\text{-}P}} = 0.25\ \sigma$ and $r_{\mathrm{const,NP\text{-}NP}} = 0.0\ \sigma$, respectively, for all cases. In order to compare the behavior during the creation and evolution of nanovoids, the interaction between NPs and polymers is set to repulsive and/or attractive, as shown in Table 1. As the solver of the cgMD simulation, we used a parallelized version of OCTA/Cognac Ver. 7.1 [16,17].

In the product runs, we deformed the PBC box in a uniaxial direction (the x-direction) with an elongation speed of 0.002 $[1/\tau]$. The dimensions of the PBC box are $L_{\mathrm{pbc},x}(\lambda) = (1+\lambda)L_{\mathrm{pbc},x}(\lambda=0)$ for the elongation ratio λ. For a Poisson ratio of 0.4, the dimensions $L_{\mathrm{pbc},y}(\lambda)$ and $L_{\mathrm{pbc},z}(\lambda)$ in perpendicular directions are $L_{\mathrm{pbc},y}(\lambda) = (1+\lambda)^{-0.4}L_{\mathrm{pbc},y}(\lambda=0)$ and $L_{\mathrm{pbc},z}(\lambda) = (1+\lambda)^{-0.4}L_{\mathrm{pbc},z}(\lambda=0)$, respectively. Note that a Poisson ratio of 0.4 is smaller than that of actual PNCs (0.46) in order to develop analysis methods in advance of large-scale cgMD simulations. We considered a Poisson ratio of 0.4 to be reasonable to consider analyses of cgMD simulations of elongated PNCs.

We prepared the initial configurations for cgMD simulations as follows: The positions of nanoparticles are given by a certain hard sphere configuration. This corresponds to a well-dispersed configuration. We set polymer melts of 640 chains of $N = 1024$ segments per chain in the space, except for the NPs in the box under the PBC. Here, we performed Monte Carlo simulation of bond fluctuation model (BFM)[18] with adding new segment to both ends until number of segments in a chain becomes $N = 1024$, where used initial configuration is randomly distributed trimers [19,20]. The reason of use of the BFM simulation for the case with existence of NPs is that double bridge method [21–23] is out of scope because target value of end-to-end length of phantom chains cannot be determined. For the case without NPs, mean square internal distance (MSID) from the BFM is similar to that of long cgMD runs by

Table 1
List of used interaction parameters. "Attractive" is the case with attractive interactions for NP-polymer and NP-NP. "Repulsive" is the case with repulsive interaction for NP-polymer and attractive interaction for NP-NP. "Repulsive(+Repulsive)" is the case with repulsive interactions for NP-polymer and NP-NP.

	Attractive NP-P	Repulsive NP-P	Repulsive NP-P (+Repulsive NP-NP)
$r_{c,P\text{-}P}$	2.5 σ	2.5 σ	2.5 σ
$r_{c,NP\text{-}P}$	2.5 σ	1.12246 σ	1.12246 σ
$r_{c,NP\text{-}NP}$	2.5 σ	2.5 σ	1.12246 σ

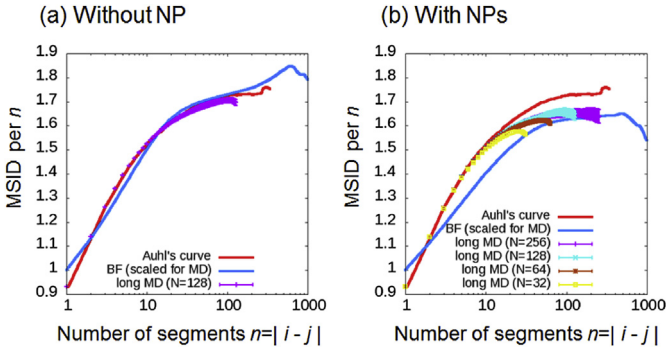

Fig. 1. Mean square internal distance (MSID) of each polymer chain produced by Monte Carlo simulations with bond fluctuation model (BFM) and cgMD simulations. For the cases without NP, MSID of the BFM for large $|i-j|$ is in good agreement with results of long MD simulation of $N = 128$. For the cases with NPs, MSID of the BFM for large $|i-j|$ seems to be reasonable by comparison with systematic behaviors of long cgMD for $N = 32$, 64, 128, and 256. Here, the Auhl's curve was read from a figure in the reference by Auhl et al. [23].

Auhl et al. [23] as shown in Fig. 1 (a). As a preliminary investigation, we estimated error bar of MSID of long cgMD runs for $N = 128$ by massive parallel computing using Large-scale Atomic/Molecular Massively Parallel Simulator (LAMMPS) [24]. Here, statistical averages are calculated after equilibration runs longer than 3 times of slowest relaxation time. In these cgMD simulations, same PBC size is used: 6400 chains for $N = 128$. It is found that error bar becomes larger for larger $|i-j|$. From the viewpoints of the MSID, the BFM seems to be good approximation for $N < 300$. For $N > 300$, we considered that behavior of the MSID of the BFM is within acceptable errors because we introduced crosslinks later. For the case with NPs, Fig. 1 (b) shows behaviors of MSID of the BFM for $N = 1024$ and long cgMD runs for $N = 32$, 64, 128, and 256 with fixed positions of NPs. From the MSID for larger $|i-j|$, the BFM seems to be reasonable. On the other hands, MSID for $|i-j| < 64$ is different from results of long cgMD simulations. It is found that in long cgMD simulations, MSID for $|i-j| < 10$ is independent from the existence of NPs. These results indicate that dependence on molecular models can be seen for small $|i-j|$. Therefore, we used the BFM in order to generate initial configurations of polymer chains of $N = 1024$. It is noted that details of efficiency of use of the BFM should be examined in future. After equilibration of polymer melts with fixed positions of NPs, we set crosslinks among different polymer chains. We examined seven numbers of crosslinks: 0, 7,072, 10,608, 14,144, 17,680, 21,216, and 42,432 bonds. These are labeled as CR0, CR1, CR1.5, CR2, CR2.5, CR3, and CR6 for simplicity. Here, the number of bonds for CR1 and CR6 is about 1% and 6% of the number of bonds of polymer melts before setting crosslinks, respectively.

3. Results & discussion

We performed cgMD simulations of PNCs constantly stretching with a Poisson ratio of 0.4. We compared two cases with repulsive and attractive interactions between polymers and NPs. To clarify the dependence on the crosslink density, we examined seven kinds of density for the attractive cases and four kinds for the repulsive cases. We should note that the deformation of crosslinked polymers is an entropy driven phenomenon and dependence of stress-strain curve on elongation speed are not negligibly small in current MD simulations because of computational limits. However, we considered that comparison among crosslink density and interaction of NP-polymer, which act as crosslinks, is effective under the condition of constant elongation speed. Fig. 2 shows stress-strain curves for various crosslink densities and interactions. For a larger crosslink density, a more rapid increase in stress can be found, indicated by an increasing elongation ratio λ. The values of stress with an attractive NP-polymer interaction are slightly larger than those with a repulsive NP-polymer interaction for high strain regions. We considered that the reason of the slight difference is that attractive NPs act as crosslinks. In the case of CR6, breakdowns of cgMD simulations are observed around $\lambda = 200\%$ because of the limitation in the length of stretched bonds. In small strain regions, the difference in stress between the two figures seems to be small. Crosslink density is considered a primary factor in stress-strain relations.

Owing to elongation with Poisson ratio 0.4, nanovoids are created and growing with the Ostwald ripening picture with increasing elongation ratio. Dynamics of growth of nanovoids becomes slower with increasing size of nanovoids. The present paper focus on effect of NP-polymer interactions and crosslink densities on fracture behaviors. Thus, detailed studies of changes of size of nanovoids and its distribution to confirm the Ostwald ripening picture is out of scope of the present paper. Fig. 3 shows snapshots of an elongated filled PNC at $\lambda = 200\%$. Here, red parts denote nanovoids. The red parts are estimated as isosurfaces for density field data of polymers and NPs. Here, used mesh size is 64^3 and 178 by 38 by 38 for $\lambda = 0\%$ and 200%, respectively. We counted number of cgMD particles of polymers and NPs in each mesh and added unity for meshes inside of each NP. As threshold of the isosurface, 0.5 is used. It was found that nanovoids are located in the bulk of polymers. Table 2 shows number of nanovoids, average mesh-counts of nanovoids, and maximum of mesh-counts of nanovoids. In the case of CR6, increase in number of nanovoids and decrease in volume of each nanovoid can be observed. Snapshots at $\lambda = 300\%$ are presented in Fig. 4. From Table 3, we can see increase in number of nanovoids and decrease in volume of each nanovoid for CR3.

In this study, the structure and dynamics of nanovoids are analyzed by using the number of voids and tunnels. Here, a tunnel is defined as a void wrapping the PBC box. To count the number of voids and tunnels, we estimated the Betti numbers (β_0, β_1, β_2, β_3) by using the CHomP software package [25] based on computational homology [26]. It should be noted that this mathematics tool is widely used to identify phase separated polymer systems in unit cells. One of the authors (K. H.) has used CHomP in previous work to study a double gyroid structure [27] whose Betti number is (β_0, β_1) = (2, 10). Here, β_0 is the number of concatenated components and β_1 is the number of independent tunnels. For example, (β_0, β_1) = (1, 0) for a single sphere and (β_0, β_1) = (1, 1) for a rod wrapping

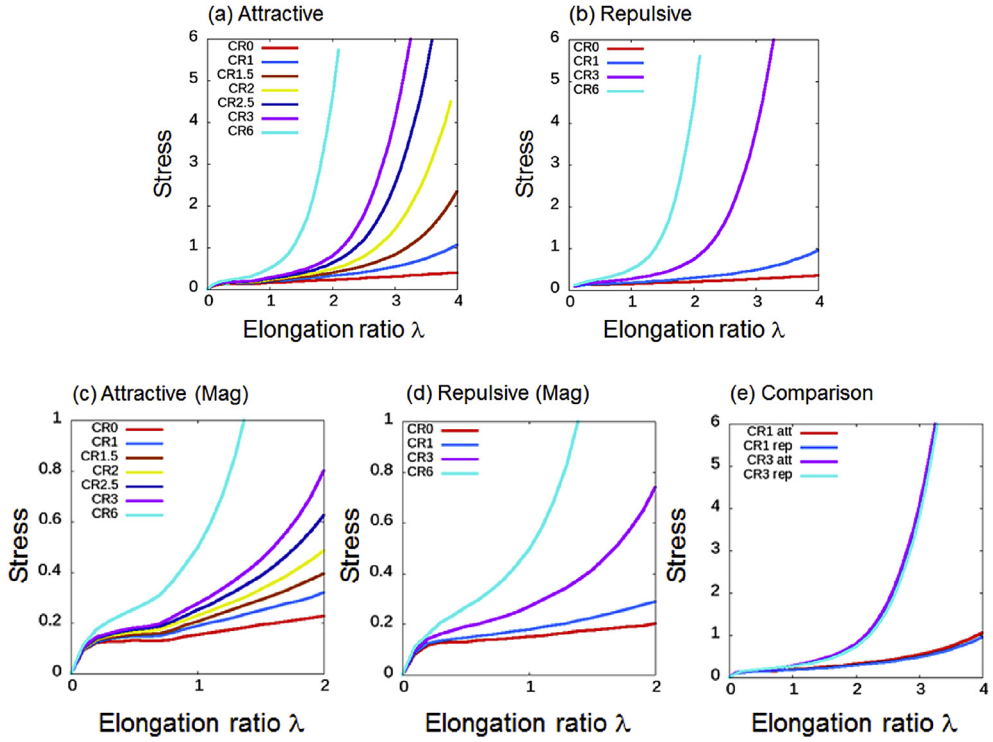

Fig. 2. Stress-strain curve with attractive and repulsive NP-polymer interactions. (a) cases with attractive NP-polymer interaction, (b) cases with repulsive NP-polymer interaction, (c) magnified view of (a), (d) magnified view of (b), and (e) Comparison among cases with attractive and repulsive NP-polymer interactions for CR1 and CR3.

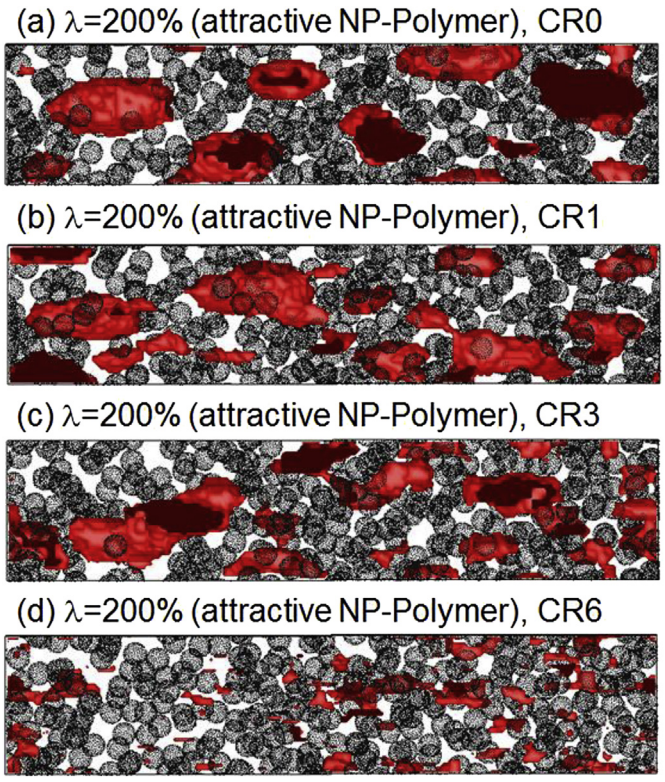

Fig. 3. Snapshot of Poisson ratio $\nu = 0.4$ with attractive NP-polymer interaction for $\lambda = 200\%$. Shapes of nanovoids depend on crosslink density. For larger crosslink density, number of nanovoids and averaged volume of each nanovoid becomes larger and smaller, respectively.

Table 2
List of number of nanovoids, average mesh-counts of each nanovoids, and maximum of mesh-counts of nanovoids for CR0, CR1, CR3, and CR6 with $\lambda = 200\%$. For larger crosslink density, number of nanovoids and averaged volume of each nanovoid becomes larger and smaller, respectively.

	CR0	CR1	CR3	CR6
Num. of voids	15	16	16	92
Ave. counts	1279.7	1098.6	890.4	35.57
Max of counts	4251	4650	4616	685

in the z-direction. In the present paper, we considered the binary fields of voids, the red parts shown in Figs. 2 and 3. According to computational homology, voids are equal to clusters in the density field and tunnels are equal to the torus of a cluster wrapping the PBC box.

Fig. 5 shows changes in Betti numbers β_0 and β_1 during elongation for the cases with attractive interactions. The change in number of voids for a small density of crosslinks along λ is quite different from that for a large density of crosslinks. For a small density of crosslinks, the number of voids converges to seven or eight at a larger λ. A decrease in the number of voids is considered to be caused by unions of voids with a rearrangement of the positions of NPs and polymers. This behavior is evidence of a cohesive fracture. Since this coalescence is related to the relaxation dynamics of PNCs, we expected it to depend on the elongation speed and system size. Detailed examinations of this are required in the future. On the other hand, for a large crosslink density, the number of voids shows a minimum as a function of the elongation ratio λ. We considered the increase in the number of voids for the high strain region originated from the division of each void due to reduction in volume of the void by surrounding NPs and crosslink networks. An increase in the number of tunnels is considered to be

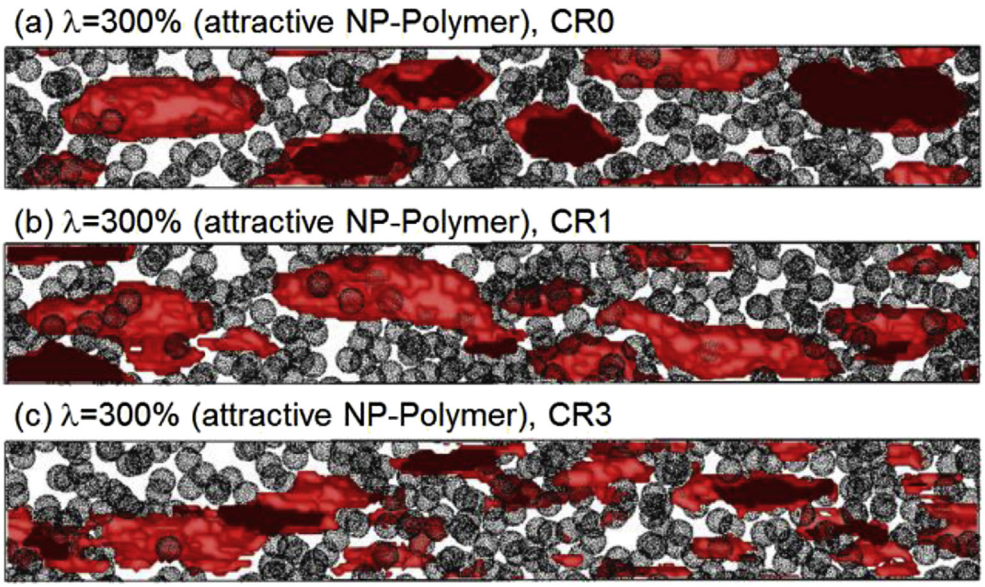

Fig. 4. Snapshot of Poisson ratio ν = 0.4 with attractive NP-polymer interaction for λ = 300%. For the case of CR3, number of nanovoids and averaged volume of each nanovoid is larger and smaller than the others.

Table 3
List of number of nanovoids, average mesh-counts of each nanovoids, and maximum of mesh-counts of nanovoids for CR0, CR1, and CR3 with λ = 300%. For the case of CR3, number of nanovoids and averaged volume of each nanovoid is larger and smaller than the others.

	CR0	CR1	CR3
Num. of voids	9	10	38
Ave. counts	3324.6	2747.9	335.8
Max of counts	6334	7787	4374

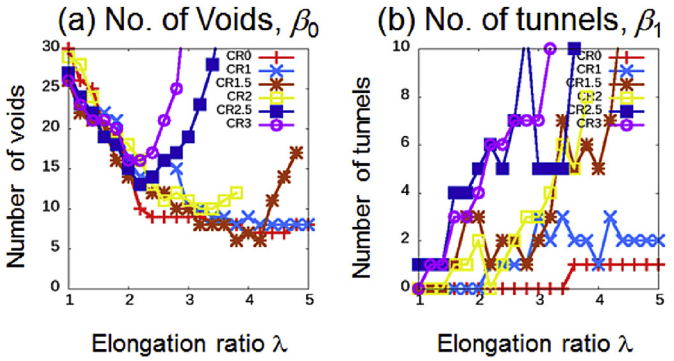

Fig. 5. Betti numbers for the case with attractive NP-polymer interaction. (a) Number of voids, β_0, and (b) number of tunnels, β_1. For larger crosslink density, number of nanovoids becomes larger. We found that number of tunnels depends on crosslink density. It is considered to be due to the formation of complicated network structures of concentrated voids owing to the splitting of small voids.

related to the formation of complicated network structures of concentrated voids owing to the splitting of small voids.

On the other hand, in the case of the repulsive NP-polymer interactions shown in Figs. 6–8, different nanovoid behaviors can be found, in which nanovoids evolve from the surface of NPs. From Figs. 6 and 7, the total volume of the voids (red parts) seems to be smaller than that for the case with an attractive NP-polymer interaction. The reason is that small voids, which are smaller than

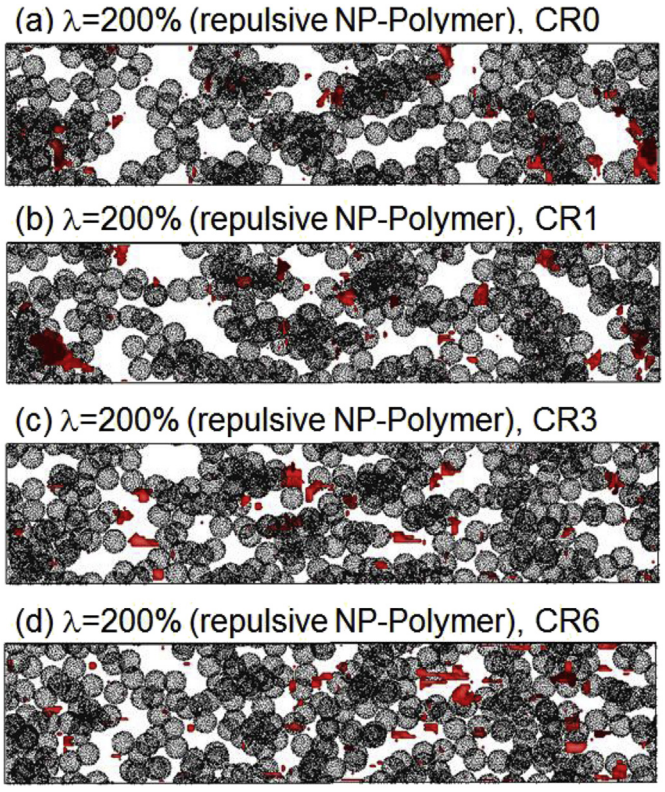

Fig. 6. Snapshot of Poisson ratio ν = 0.4 with repulsive NP-polymer interaction for λ = 200%. Nanovoids are created at the interface between NPs and polymers. The grown nanovoids are located at interfaces between NPs and polymers. Differences of crosslink density seem to be small in comparison with the cases with attractive NP-polymer interaction.

the gap size between neighboring NPs, are hard to detect as voids using mesh and an algorithm from particles to mesh. In Fig. 8, the number of voids increases with a small λ, and it becomes constant with a large λ. A large number of voids indicates an interfacial

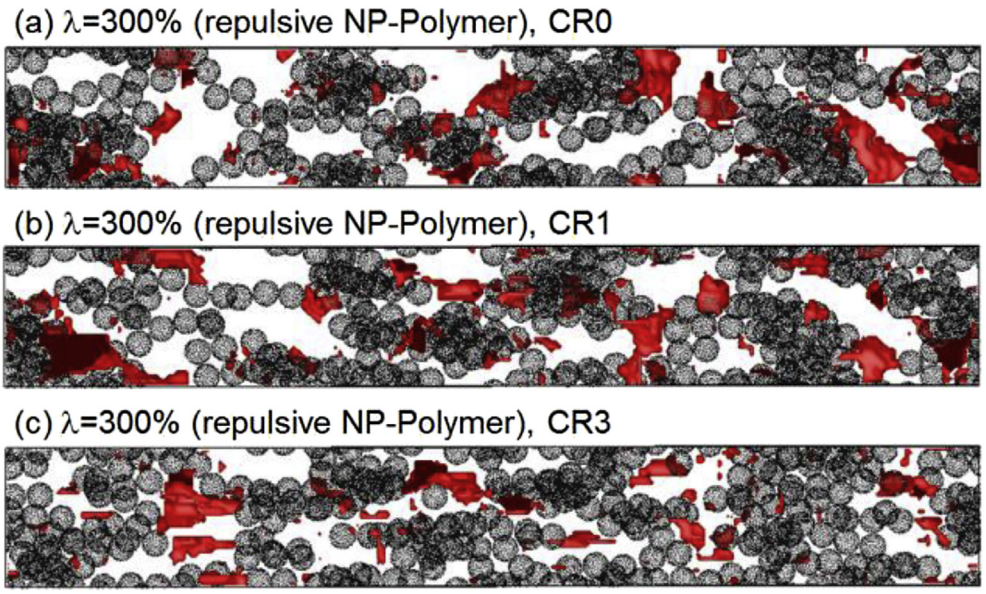

Fig. 7. Snapshot of Poisson ratio $\nu = 0.4$ with repulsive NP-polymer interaction for $\lambda = 300\%$. Differences of crosslink density on shapes of nanovoids are observed. For the case of CR3, size of nanovoids is smaller than that of the others. For the cases with crosslinks (CR1 and CR3), strings of NPs can be seen.

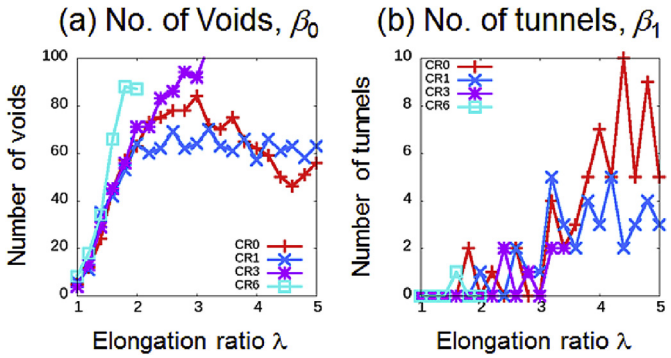

Fig. 8. Betti numbers for the case with repulsive NP-polymer interaction. (a) Number of voids, β_0, and (b) number of tunnels, β_1. For the case of CR3, number of voids is larger than that of CR0 and CR1. It indicates that averaged size of nanovoids is smaller than that of CR0 and CR1.

fracture and trapping of voids at NP gaps. The number of tunnels increases to over $\lambda = 300\%$. From these behaviors, we considered that a coalescence of voids does not occur. At the same time, we observed the progression of NP segregation and the characteristic behavior that NPs form a line along an extension direction, which can clearly be found in Fig. 7 for $\lambda = 300\%$. We supposed that the reason for formation of a line of NPs is the attractive interaction between NPs and/or confinements by the crosslinked polymer network. To confirm our supposition, we performed additional cgMD simulations under the conditions of repulsive NP-polymer interaction and repulsive NP-NP interaction. In Fig. 9, the snapshots of three kinds of simulations with the parameters given in Table 1 are shown. From Fig. 9 (e) and (f), strings of NPs can be observed regardless of the NP-NP interaction, although those cannot be found in the case of zero crosslinks shown in Fig. 9 (b) and (c). In the case of attractive NP-polymer interaction, we can see large nanovoids and cannot observe strings of NPs as shown in Fig. 9 (a) and (d). Thus, we concluded that the important factors for formation of a line of NPs are segregation of NPs, i.e., both repulsive NP-polymer interaction and confinement by the surrounding crosslinked network. In addition, for the cases of repulsive NP-polymer interaction, observed size of nanovoids in Fig. 9 (c) and (f), that are the cases with repulsive NP-NP interaction, is smaller than that in Fig. 9 (b) and (e), that are the cases with attractive NP-NP interaction. We expected that small nanovoids are generated at spaces among NPs for the cases with repulsive NP-NP interaction.

4. Summary and conclusion

We performed coarse-grained molecular dynamics simulations of crosslinked polymer chains filled with spherical nanoparticles under elongation with a Poisson ratio of 0.4 in order to study the effects of interactions on fracture modes and develop numerical analysis schemes. When a NP-polymer interaction is attractive or repulsive, a cohesive or interfacial fracture is observed, respectively. For the case of an attractive NP-polymer interaction, nanovoids appear in the bulk of polymers, and the nanovoids grow with fusions. Due to the existence of crosslinks, the growth is limited. In addition, for a high strain region, deformed polymer networks with crosslinks split nanovoids into small fragmentations. Thus, we concluded that the cohesive fractures occur in the case with attractive NP-polymer interactions. On the other hand, for the case with repulsive NP-polymer interactions, voids were born at the interface between polymers and NPs. It can be concluded that this fracture mode is an interfacial fracture. Moreover, we found that the deformed crosslink networks form strings of NPs. We expect that this predicted behavior can be observed in real-space experiments with 3D-TEM [28], FIB-SEM [29], in inverse-space experiments with small-angle X-ray scattering and reverse Monte Carlo modeling [30], and/or with hybrid math-based analysis [31] combining data from the above experiments. The behavior of the scattering patterns of filled rubbers under stretching are also very interesting, as reported by Zhang et al. [13]. To reproduce these phenomena in cgMD simulations, a realistic Poisson ratio (about 0.46), diameter distribution of NPs, and contrast among polymers and NPs should be taken into account. Detailed studies in these directions are in progress.

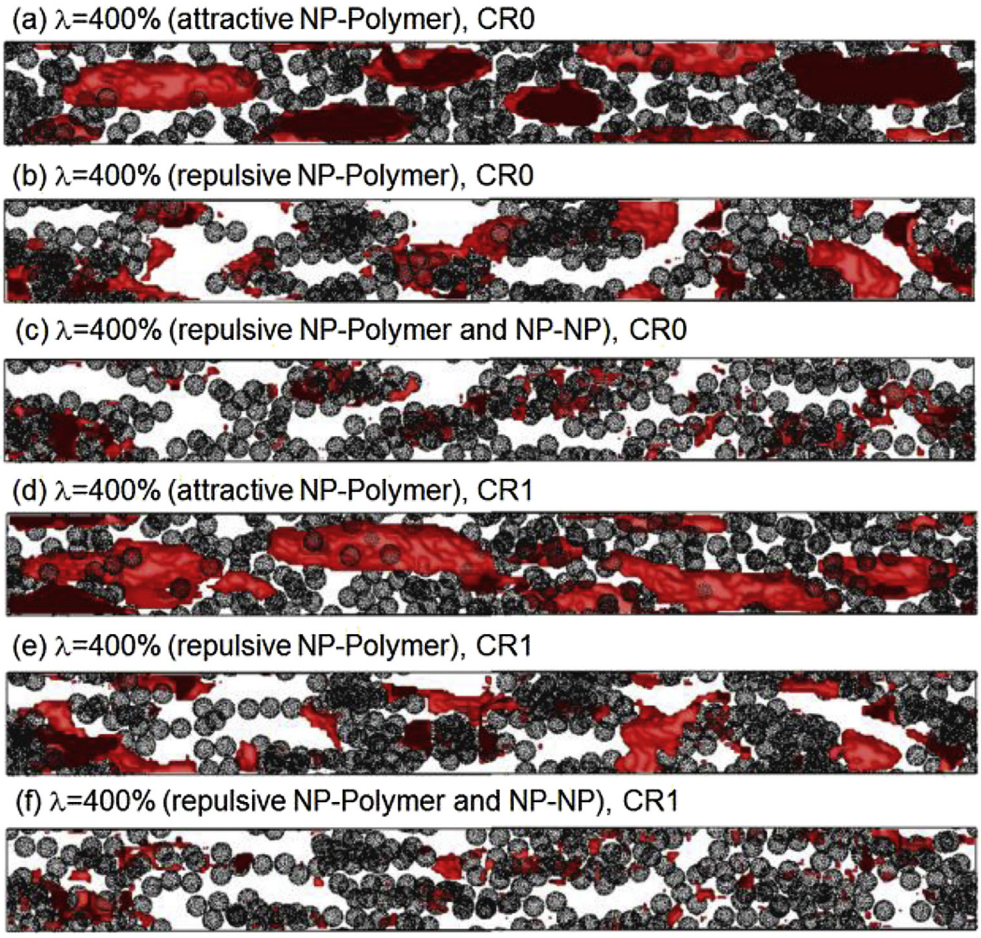

Fig. 9. Snapshots with CR0 and CR1 for $\lambda = 400\%$. By comparing (c) with (e) and (f), it can be seen that strings of NPs appear for the case with crosslinks. We expected that crosslinked network due to existence of crosslinks restrict global movements of NPs. For the cases of repulsive NP-polymer interaction, size of nanovoids with repulsive NP-NP interaction is smaller than that with attractive NP-NP interaction.

Author contributions

The manuscript was written through contributions of all authors. Computation and analysis are mainly performed by K.H. All authors have given approval to the final version of the manuscript.

Acknowledgment

The authors thank Prof. M. Doi for their useful discussions. We would like to thank Prof. M. Omiya, Dr. Y. Hirose, Dr. N. Goda, and Dr. T. Aoyagi for the SMP-parallelized version of OCTA/COGNAC at the Information Initiative Center, Hokkaido University. One of the author (K.H.) acknowledges Dr. T. Teramoto for discussions and collaborations about computational homology and its mathematical tools. The authors are partially supported by the Joint Usage/Research Center for Interdisciplinary Large-scale Information Infrastructures (JHPCN) and the High-Performance Computing Infrastructure (HPCI) in Japan.

References

[1] T.A. Vilgis, G. Heinrich, M. Klüppel, Reinforcement of Polymer Nano-composites, 2009. Cambridge.
[2] J.E. Mark, B. Erman, M. Roland, The Science and Technology of Rubber, fourth ed., Academic Press, 2013.
[3] Q.H. Zeng, A.B. Yu, G.Q. Lu, Multiscale modeling and simulation of polymer nanocomposites, Prog. Polym. Sci. 33 (2008) 191–269.
[4] G. Allegra, G. Raos, M. Vacatello, Theories and simulations of polymer-based nanocomposites: from chain statistics to reinforcement, Prog. Polym. Sci. 33 (2008) 683–731.
[5] C. Chevigny, F. Dalmas, E.D. Cola, D. Gigmes, D. Bertin, F. Boué, J. Jestin, Polymer-grafted-nanoparticles nanocomposites: dispersion, grafted chain conformation, and rheological behavior, Macromolecules 44 (2011) 122.
[6] D. Zhao, M.D. Nicola, M.M. Khani, J. Jestin, B.C. Benicewicz, S.K. Kumar, Self-assembly of monodisperse versus bidisperse polymer-grafted nanoparticles, ACS Macro Lett. 5 (2016) 790.
[7] P. Akcora, H. Liu, S.K. Kumar, J. Moll, Y. Li, B.C. Benicewicz, L.S. Schadler, D. Acehan, A.Z. Panagiotopoulos, V. Pryamitsyn, V. Ganesan, J. Ilavsky, P. Thiyagarajan, R.H. Colvy, J.F. Douglas, Anisotropic self-assembly of spherical polymer-grafted nanoparticles, Nat. Mat. 8 (2009) 354.
[8] A.N. Gent, B. Park, Failure processes in elastomers at or near a rigid spherical inclusion, J. Mater. Sci. 19 (1984) 1947–1956.
[9] D. Hull, T.W. Clyne, An Introduction to Composite Materials, Cambridge University Press, 1996.
[10] S. Wu, Polymer Interface and Adhesion, Marcel Dekker, Inc, 1982.
[11] T. Yamaguchi, H. Morita, M. Doi, Modeling on debonding dynamics of pressure-sensitive adhesives, Eur. Phys. J. E. 20 (2006) 7–17.
[12] T. Yamaguchi, K. Koike, M. Doi, In situ observation of stereoscopic shapes of cavities in soft adhesives, Eur. Phys. Lett. 7 (2007). 64002-p1-p5.
[13] H. Zhang, A.K. Scholz, J.C.F. Vion-Loisel, G. Besnard, A. Hexemer, H.R. Brown, E.J. Kramer, C. Creton, Nanocavitation in carbon black filled styrene–butadiene rubber under tension detected by real time small angle X-ray scattering, Macromolecules 45 (2012) 1529–1543.
[14] K. Hagita, M. Morita, M. Doi, H. Takano, Coarse-grained molecular dynamics simulation of filled polymer nanocomposites under uniaxial elongation, Macromolecules 49 (2016) 1972–1983.
[15] K. Kremer, G.S. Grest, Dynamics of entangled linear polymer melts: a molecular-dynamics simulation, J. Chem. Phys. 92 (1990) 5057–5086.
[16] T. Aoyagi, F. Sawa, T. Shoji, H. Fukunaga, J. Takimoto, M. Doi, A general-purpose coarse-grained molecular dynamics program, Comput. Phys. Comm. 145 (2007) 267–279.
[17] http://octa.jp/.

[18] I. Carmesin, K. Kremer, The bond fluctuation method: a new effective algorithm for the dynamics of polymers in all spatial dimensions, Macromolecules 21 (1988) 2819.
[19] N.C. Karayiannis, V.G. Mavrantzas, D.N. Theodorou, A novel monte carlo scheme for the rapid equilibration of atomistic model polymer systems of precisely defined molecular architecture, Phys. Rev. Lett. 88 (2002) 105503.
[20] N.C. Karayiannis, A.E. Giannousaki, V.G. Mavrantas, D.N. Theodorou, Atomistic Monte Carlo simulation of strictly monodisperse long polyethylene melts through a generalized chain bridging algorithm, J. Chem. Phys. 117 (2002) 5465.
[21] R. Auhl, R. Everaers, G.S. Grest, K. Kremer, S.J. Plimpton, Equilibration of long chain polymer melts in computer simulations, J. Chem. Phys. 119 (2013) 12718.
[22] K. Hagita, H. Takano, Relaxation mode analysis of a single polymer chain in a melt, J. Phys. Soc. Jpn. 71 (2002) 673.
[23] K. Hagita, H. Takano, Self-diffusion of a polymer chain in a melt, J. Phys. Soc. Jpn. 72 (2003) 1824.
[24] S. Plimpton, Fast parallel algorithms for short-range molecular dynamics, J. Comp. Phys. 117 (1995) 1.
[25] Kalies W.; Pilarczyk, P. Computational Homology Project. http://chomp.rutgers.edu/.
[26] T. Kaczynski, K. Mischaikow, M. Morzek, Computational Homology, Applied Mathematical Sciences, Springer-Verlag, NewYork, 2004, p. 480. No. 157.
[27] K. Hagita, T. Teramoto, Topological validation of morphology modeling by extended reverse Monte Carlo analysis, Phys. Rev. E. 77 (2008) 056704.
[28] H. Jinnai, Y. Shinbori, T. Kitaoka, K. Akutagawa, N. Mashita, T. Nishi, Three-dimensional structure of a nanocomposite material consisting of two kinds of nanofillers and rubbery matrix studied by transmission electron. Microtomography, Macromolecules 40 (2007) 6758–6764.
[29] M. Kato, T. Ito, Y. Aoyama, K. Sawa, T. Kaneko, N. Kawase, H. Jinnai, Three-dimensional structural analysis of a block copolymer by scanning electron microscopy combined with a focused ion beam, J. Polym. Sci. Part B Polym. Phys. 45 (2007) 677–683.
[30] K. Hagita, T. Tominaga, T. Sone, Large scale reverse Monte Carlo analysis for ultra small angle x-ray scattering data of silica nanoparticles in end-modified rubbers, Submitt. Phys. Rev. E (2016).
[31] Jinnai, H.; Hagita, K. Super-resolution technique for 3d-TEM and FIB-SEM with supporting scattering data. Priv. Commun.